

# Superposition of photon and phonon assisted tunneling in coupled quantum dots

H. Qin, A.W. Holleitner, K. Eberl<sup>†</sup>, and R.H. Blick

Center for NanoScience and Sektion Physik, Ludwig-Maximilians-Universität, Geschwister-Scholl-Platz 1, 80539 München, Germany.

<sup>†</sup> Max-Planck-Institut für Festkörperforschung, Heisenbergstr. 1, 70569 Stuttgart, Germany.  
(December 2, 2024)

We report on electron transport through an artificial molecule formed by two tunnel coupled laterally gated quantum dots. The dots are of medium size containing roughly 200 electrons per dot. We find photon-assisted tunneling (PAT) of electrons through the double dot and probe the coherent molecular states by tuning the tunnel coupling between the dots. In addition, we observe PAT mediated by acoustic phonons below a threshold microwave frequency of around 8 GHz. The quantum dots are coupled coherently, absorbing microwave photons and acoustic phonons.

73.23.Hk;85.30.Vw;03.67.Lx

Coupled quantum dots allow to form an artificial molecule in which the onset of coherent electronic modes can be monitored [1]. This coherent state can be probed either by transport or microwave spectroscopy [2,3]. Studying the interaction of few-electron systems with distinct phonon modes is of great importance, since this will allow to tailor the dissipation processes in these nanostructures. Moreover, coupled dots were proposed as possible candidates for realizing quantum bits in solid state systems [4]. Obviously, one of the obstacles for such an application is the considerable dephasing induced by the environment. Since double dot molecules are fabricated in semiconductor host materials they are coupled to the electromagnetic and the thermal environment which leads to dephasing. Recently, Fujisawa *et al.* [5] found that vacuum fluctuations induce pronounced transitions between energetically well-separated quantum levels, generating discrete phonon modes in quantum dots. A detailed theoretical investigation was presented by Brandes and Kramer [6].

We present transport measurements on a double dot molecule coupled to both microwave photons and acoustic phonons. We probe the formation of molecular states through one-photon and two-photon PAT processes as demonstrated experimentally [3] and theoretically modeled before [7,8]. In addition, we present the combination of PAT with phonon-assisted tunneling. We verify the persistence of coherent molecular states in a double quantum dot under both phonon and photon excitations.

As shown in Fig. 1(a), five pairs of Schottky gates are defined by electron beam lithography forming a coupled double quantum dot in a two-dimensional electron system (2DES) located 90 nm below the surface of an Al-GaAs/GaAs heterostructure. At 4.2 K the carrier density of the 2DES is  $1.7 \times 10^{15} \text{ m}^{-2}$  and the electron mobility is  $80 \text{ m}^2/\text{Vs}$ . Both dots have an effective electronic diameter  $d$  of about 500 nm. The 2DES is cooled down to a bath temperature  $T_b$  of 170 mK in a  $^3\text{He}/^4\text{He}$  dilution refrigerator. To couple the microwave radiation to the quantum dot, we use a Hertzian wire-loop antenna

about 1 cm above the dots [9].

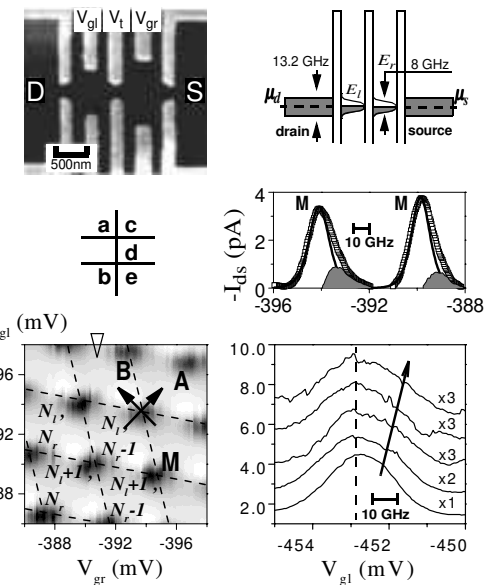


FIG. 1. (a) The scanning electron microscope graph of this double dot. (b) Charging diagram of drain-source current with weak tunnel coupling ( $G_c \sim 0.08 \text{ e}^2/\text{h}$ ) (white:  $I_{ds} \sim 0 \text{ pA}$ , black:  $I_{ds} \sim -4 \text{ pA}$ ). (c) the level diagram illustrates the resonant tunneling and the temperature broadening in the leads and dots. (d) A single trace extracted from (b) at a constant  $V_{gr}$  marked by the open triangle. (e) Temperature dependence of the peak asymmetry in the tunneling through the double dot. The bath temperatures are 276 mK, 320 mK, 468 mK, 564 mK and 634 mK for the curves from bottom to top, respectively.

For tuning the double dot into the tunnel coupling regime [10], the tunneling rates of two outer tunnel barriers are kept fixed around  $\Gamma_L^{-1} \sim \Gamma_R^{-1} \sim 2 \text{ nsec}$  and the tunnel conductance  $G_c$  of the center barrier is controlled by  $V_t$  (see Fig. 1(a)). The dots contain around 200 electrons each and show excited states at  $\Delta\epsilon^* \cong 120 \text{ } \mu\text{eV}$  above the ground state. The effective calibration factors ( $\alpha_l$  and  $\alpha_r$ ) are  $6.8 \times 10^{-2}$  and

$5.2 \times 10^{-2}$  for the left and right dot, respectively [11]. From the charging diagrams of the drain-source current  $I_{ds}$  we find the charging energies [12] ( $U_l$  and  $U_r$ ) of  $391 \mu\text{eV}$  and  $318 \mu\text{eV}$ . The electron temperature in the leads ( $T_e \cong 180 \text{ mK}$ ) is obtained simply by measuring the full-width-at-half-maximum of the conductance of a single quantum dot [13,14]. In the measurements shown below, we operate the double dot in the linear transport regime, i.e. the drain-source bias  $V_{ds}$  is fixed at around  $-10 \mu\text{V} \ll \Delta\epsilon^*/e$ . With negative  $V_{ds}$  electrons tunnel through the double dot from the drain to the source. In Fig. 1(b) the charging diagram of the coupled dot is plotted in a grayscale representation in the weak coupling regime ( $G_c \sim 0.08 e^2/h$ ). The discrete conductance peaks in Fig. 1(b) are main peaks **M** resulting from resonant tunneling through the double dot (see Fig. 1(c)). Within the diamond shaped regions enclosed by dashed lines Coulomb blockade prevails and the number of electrons in the dots is well defined.

In the direction marked by arrow **A**, the relative level distance  $E_{lr} = -(E_l - E_r)$  between two quantum dot states involved in transport is kept constant, while the average  $(E_l + E_r)/2$  is increased relative to the chemical potentials ( $\mu_d$  and  $\mu_s$ ) in the drain and source leads. In direction of **B**, where  $(E_l + E_r)/2$  is kept fixed but  $E_{lr}$  is varied, we find that the broadening is dominated by the electron temperature within the dots but not the intrinsic life time of the quantum levels. The temperature broadening in the dots ( $\hbar\Gamma$ ) is estimated to be about  $\hbar \times 8 \text{ GHz}$ , which is slightly lower than the electron temperature in the leads. In Fig. 1(c), the level diagram takes into account the temperature broadening in the leads and the dots. A typical single trace extracted from the charging diagram is shown in Fig. 1(d). On the left side of the peak, where  $E_l$  is higher than  $E_r$ , it is well approximated by  $\cosh^{-2}(\epsilon/2k_B T_e)$  (see the solid line in Fig. 1(d)). However, on the right side where  $E_l$  is lower than  $E_r$ , there exists an additional contribution to the tunneling current, which has a maximum about 12 GHz away from the main peak (see the dark area in Fig. 1(d)). By increasing the bath temperature, we find the position of this maximum shifts further to the right side, as shown in Fig. 1(e). We note that due to the background radiation and a finite electron temperature electrons absorb acoustic phonons via deformation potential coupling, i.e. at a bath temperature of  $T_b = 170 \text{ mK}$  a corresponding frequency of acoustic phonons  $f_{ph} \sim 3k_B T_b/\hbar \approx 10.7 \text{ GHz}$  is obtained.

Microwave spectroscopy on the weakly coupled dots ( $G_c \sim 0.08e^2/h$ ) is then studied by taking charging diagrams upon applying microwave radiation in the range of 1–20 GHz. The electron temperature is slightly increased to be  $T_e \approx 210 \text{ mK}$  in the leads (see also Fig. 4(a)), but the peak position of the sidebands is independent of microwave power applied. The charging diagrams at 20 GHz and 3 GHz are shown in Fig. 2. In

the grayscale plot of Fig. 2(a) the double dot shows a regular pattern of resonances. Peaks bound to the main peak **M** are the microwave induced sidebands at 20 GHz. For clarification a single trace taken out of the charging diagram (position indicated by the dashed line) is plotted in the right panel of Fig. 2(a). Clearly, we observe one- and two-photon absorption processes marked by **P**<sub>1</sub> and **P**<sub>2</sub>. Below 10 GHz only one sideband **S** is clearly observed (see Fig. 2(b), only the data for 3 GHz are shown) and most strikingly the distance between **M** and **S** is comparable to that at 20 GHz or even larger. Furthermore, under microwave radiation at 3 GHz, 4.5 GHz, and 5.9 GHz an additional tunneling current **X** located in between **M** and **S** is observed, as shown in the single traces in Fig. 2(b).

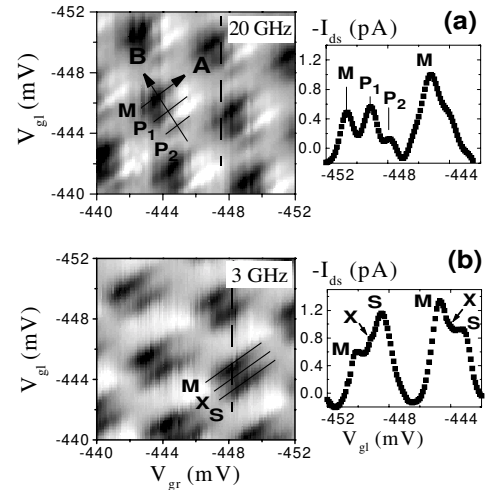


FIG. 2. Charging diagrams with microwave radiation at (a) 20 GHz and (b) 3 GHz (white:  $I_{ds} \sim 0 \text{ pA}$ , black:  $I_{ds} \sim -4 \text{ pA}$ ). The single traces from the grayscale plot show the details. See text for details on symbols **P**<sub>1</sub>, **P**<sub>2</sub>, **S** and **X**.

In Fig. 3(a), the distance between the sidebands (**P**<sub>1</sub>, **P**<sub>2</sub>, **X** and **S**) and the main peak (**M**), converted from gate voltages  $\Delta V_{gl,gr}$  to energies  $E_{lr}$  using the factors  $\alpha_{l,r}$ , are plotted over the microwave frequency applied. Above 10 GHz the distance is equal to the corresponding microwave photon energies  $hf$  and  $2hf$  as described by the Tien-Gorden theory [15]. Below 8 GHz, however, the distance for sidebands **X** and **S** follow

$$E_{lr}^X = h(f + f_0), \quad (1)$$

$$E_{lr}^S = 2h(f + f_0), \quad (2)$$

respectively, with an offset  $f_0 \approx 10 \text{ GHz}$ . Apart from the offset, the slopes of the traces correspond to the absorption of one and two photons. Hence, we have to consider an additional absorption mechanism leading to the offset  $hf_0$  and  $2hf_0$ . Moreover, it has to be noted that the

hatched area in Fig. 3(a) marks a transition region between 8 GHz and 10 GHz. As schematically shown in Fig. 4, the two states involved in transport are, e.g. the  $N_l$ th ground state in the left dot and the  $N_r$ th ground state in the right dot.

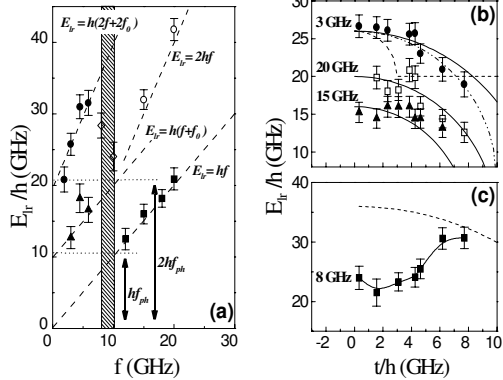


FIG. 3. (a) The distance between the side band and the main peak versus the microwave frequency in the weak tunnel coupling regime ( $G_c \sim 0.08 e^2/h$ ).  $f > 10$  GHz: Solid squares and open circles are for sidebands  $\mathbf{P}_1$  and  $\mathbf{P}_2$ , respectively.  $f < 8$  GHz: Solid circles and solid triangles stand for sidebands  $\mathbf{S}$  and  $\mathbf{X}$ , respectively. In the hatched region (8 GHz - 10 GHz), the open diamonds corresponds to sidebands  $\mathbf{S}$ . (b) The coupling dependence of the distance between the side bands and the main peak at 20 GHz, 15 GHz, and 3 GHz. For 20 GHz and 15 GHz, the solid lines corresponds to eq. [3]. For 3 GHz, the dashed line is from eq. [4], the dash/dotted line is fitted with eq. [5], and the solid line is based on eq. [6]. (c) At 8 GHz, the dashed curve is calculated from eq. [6].

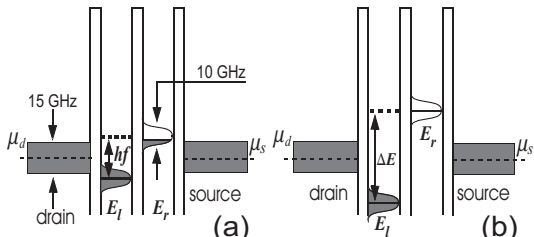


FIG. 4. Level diagrams for (a) one-photon PAT with microwave frequencies above 10 GHz, and (b) transport with microwave frequencies below 8 GHz.

In order to distinguish the different nature of these sidebands and the offset  $h f_0$  and  $2 h f_0$ , we vary the coupling strength between the dots through adjusting the center gate voltage and measuring the energetic distance of sidebands to the main peak. The data are shown in Fig. 3(b,c). The variation of the tunnel coupling enables us to trace the transition of the artificial molecule from 'ionic' to 'covalent' binding by determining the peak splitting  $E_r$ . We find that at 20 GHz and 15 GHz the peak distance from  $\mathbf{P}_1$  to  $\mathbf{M}$  can be roughly fitted by

$$E_{lr}^{P_1} = \sqrt{(h f)^2 - 4 t^2}, \quad (3)$$

where  $t$  is the tunnel coupling strength between the two dots and we simply assume it is proportional to the coupling conductance:  $t \propto G_c$ . Eq. [3] is a signature of a coherently coupled two-level system as studied before [3,7,8]. This implies that the two dots are coupled coherently and form an artificial molecule. The resonance of this molecular state is driven by the microwave radiation, which matches the resonance frequency.

Commonly, one expects a similar photon coupling below 10 GHz as described by eq. [3]. The coupling dependence obtained turns out to be quite different: An increase of the tunnel coupling at  $f = 8$  GHz enhances the splitting (see Fig. 3(c)). At  $f = 3$  GHz, the coupling then again follows similar traces as those at 20 GHz and 15 GHz (see Fig. 3(b)). We assume an additional energy offset  $2 h f_0$  being involved below 8 GHz.

Since we operate the coupled dots in the regime of linear response at a bias voltage of only  $-10 \mu\text{V}$ , we can exclude electronic excitations from the drain/source leads supplying this energy. As mentioned before, the single particle excitation energies of the individual dots  $\Delta\epsilon^* \cong 120 \mu\text{eV} \approx 30 \text{ GHz}$  is larger than  $2 h f_0$ . Hence, intrinsic excitations in the dots will not interfere with molecular states and PAT below 8 GHz. The remaining source of this offset energy quantity  $2 h f_0$  is the crystal lattice in which the quantum dots are embedded. As discussed earlier by Fujisawa *et al.* [5] acoustic phonons – neither plasma excitations nor optical phonons – effectively contribute to electron transport through such a quantum dot device. Compared to this work, our double dot molecule is probed under much lower drain-source bias. As a result, no phonon emission but phonon absorption is observed. In our case, the GaAs/AlGaAs lattice is cooled by the  $^3\text{He}/^4\text{He}$  mixture at a bath temperature of  $T_b = 170 \text{ mK}$ . This yields an acoustic phonon energy of  $h f_{ph} \approx h \times 10.7 \text{ GHz}$ . Assuming a sound velocity  $v_{3D}$  of 4800 m/s in the GaAs host crystal, this 3D phonon mode has a wavelength of about 480 nm, which is comparable to the effective dot diameter  $d$  and the distance  $L$  between the centers of the two dots ( $d, L \sim 500 \text{ nm}$ ). This phonon energy also matches the level broadening within the dots, which confirms that the double-dot molecule is strongly heated by the phonon bath. Since the two quantum dots form cavities for 10 GHz phonons, the electrons strongly interact with phonons. Therefore, the energy quantum  $2 h f_0$  most likely consist of two phonons:  $2 h f_0 \approx 2 \times h f_{ph}$ .

Another possible source of phonons is the gate structure itself: Similar to interdigitated transducers (IDTs), which are commonly used to launch surface acoustic waves [16], the gates not only confine the electrons in the quantum dots but moreover form a piezoelectrical resonator. Due to the limited number of gates in comparison to conventional IDTs this 'Schottky-gate' transducer possesses a large bandwidth, i.e. exciting this transducer

far off resonance still generates phonons.

Assuming photon and phonon excitations, transport through the double dot at 3 GHz could be coherent as well as sequential. The first process to be considered is the following: A single electron is lifted into an intermediate state by absorption of phonons in one dot and then coupled to the other dot via two-photon absorption, i.e

$$E_{lr}^S = \sqrt{(2hf)^2 - 4t^2} + 2hf_0, \quad (4)$$

being depicted by the dashed curve in Fig. 3(b), which is obviously not observed. The other sequential process is given by the absorption of photons in one dot and then the phonon absorption between the dots. The corresponding coupling dependence follows

$$E_{lr}^S = \sqrt{(2hf_0)^2 - 4t^2} + 2hf, \quad (5)$$

depicted by the dashed/dotted trace in Fig. 3(b), which is in reasonable agreement with the experimental data. On the other hand, an electron tunneling coherently through the dots can absorb both photons and phonons. The coupling dependence is then written as

$$E_{lr}^S = \sqrt{(2h(f + f_0))^2 - 4t^2}, \quad (6)$$

illustrated by the solid curve in Fig. 3(b). Within the error bars also this process can be assumed, although the sequential absorption of phonons and photons (eq. [5]) obviously fits better. However, in any case it has to be pointed out that the 'molecular state' at 3 GHz is not dephased by sequentially or coherently absorbing phonons and photons. The two quantum dots can be coupled coherently by either microwave photons or acoustic phonons. In general, this can be understood as a superposition of photon *and* phonon assisted tunneling ( $\Sigma$ PAT). Above 10 GHz conventional PAT prevails, since the absorption of more than two phonons is much less likely than that of photons. In the transition region from pure PAT to  $\Sigma$ PAT, between 8 GHz and 10 GHz, transitions induced by photons and phonons are strongly mixed and no simple superposition of phonons and photons is found.

In summary, we couple two quantum dots of medium size at relatively high temperature and probe coherent electron transport by microwave spectroscopy. Apart from conventional photon-assisted tunneling (PAT), we observe a combination of photon- and phonon-assisted tunneling ( $\Sigma$ PAT). The whole tunneling process can be either coherent or sequential while the coupling between the quantum dots is found to be coherent. We verify that the coherent electronic mode formed in the coupled dots sustains the absorption of phonons formed within the quantum dots.

We like to thank W. Zwerger for helpful discussions and J.P. Kotthaus for support. This work was funded in part by the Deutsche Forschungsgemeinschaft

within the project SFB 348, the Bundesministerium für Forschung und Technologie (BMBF) with the project Quantenstrukturbauelemente (01BM914), and the Defense Advanced Research Projects Agency (DARPA) within the Ultrafast Electronics Program (F61775-99-WE015). H.Q. gratefully acknowledges support by the Volkswagen Stiftung.

---

- [1] L.P. Kouwenhoven et. al, in *Mesoscopic Electron Transport, Proceedings of a NATO Advanced Study Institute*, L.L. Sohn, L.P. Kouwenhoven and G. Schön, Eds., Kluwer, Dordrecht, ser. E, vol. 345 (1997).
- [2] R.H. Blick, D. Pfannkuche, R.J. Haug, K. von Klitzing, and K. Eberl, *Phys. Rev. Lett.* **80**, 4032 (1998); R.H. Blick, D.W. van der Weide, R.J. Haug, K. Eberl, *ibid* **81**, 689 (1998); A.W. Holleitner, C.R. Decker, K. Eberl, and R.H. Blick, *cond-mat/0011044*
- [3] T.H. Oosterkamp, T. Fujisawa, W.G. van der Wiel, K. Ishibashi, R.V. Hijman, S. Tarucha and L.P. Kouwenhoven, *Nature* **395**, 873 (1998).
- [4] D. Loss and D.P. DiVincenzo, *Phys. Rev. A* **57**, 120 (1998).
- [5] T. Fujisawa, T.H. Oosterkamp, W.G. van der Wiel, B.W. Broer, R. Aguado, S. Tarucha, and L.P. Kouwenhoven, *Science* **282**, 932 (1998); T. Fujisawa, W.G. van der Wiel, L.P. Kouwenhoven, *Physica E* **7**, 413 (2000).
- [6] T. Brandes and B. Kramer, *Phys. Rev. Lett.* **83**, 3021 (1999).
- [7] C.A. Stafford and N.S. Wingreen, *Phys. Rev. Lett.* **76**, 3455 (1996).
- [8] T.H. Stoof and Yu.V. Nazarov, *Phys. Rev. B* **53**, 1050 (1996).
- [9] H. Qin, F. Simmel, R.H. Blick, J.P. Kotthaus, W. Wegscheider, M. Bichler, *Phys. Rev. B*, in press (2001).
- [10] C. Livermore, C.H. Crouch, R.M. Westervelt, K.L. Campman, and A.C. Gossard, *Science* **274**, 1332 (1996).
- [11] The factors  $\alpha_l$  and  $\alpha_r$  are defined as  $\alpha_{l,r} = \delta E_{lr}/e\delta V_{gl,gr}$ , where  $E_{lr} = -(E_l - E_r)$  represents the level distance between the left and right dot.
- [12] For convenience, we define the charging energy ( $U_{l,r}$ ) for each dot as  $U_{l,r} = e^2/C_{\Sigma}^{l,r}$ , where  $C_{\Sigma}^l$  and  $C_{\Sigma}^r$  are the total capacitances of the left and right dot, respectively.
- [13] C.W.J. Beenakker, *Phys. Rev. B* **44**, 1646 (1991).
- [14] E.B. Foxman, P.L. McEuen, U. Meirav, N.S. Wingreen, Y. Meir, P.A. Belk, N.R. Belk, and M.A. Kastner, *Phys. Rev. B* **47**, 10020 (1993).
- [15] P.K. Tien and J.R. Gorden, *Phys. Rev.* **129**, 647 (1963).
- [16] A. Wixforth, J. Scriba, M. Wassermeier, J.P. Kotthaus, G. Weimann, and W. Schlapp, *Phys. Rev. B* **40**, 7874 (1989); A. Wixforth, private communication.